Front. Earth Sci. 2024, 18(1): 227–241
https://doi.org/10.1007/s11707-022-1062-6

RESEARCH ARTICLE

Deformation characteristics and analog modeling of transtensional structures in the Dongying Sag, Bohai Bay Basin

Dawei DONG[1], Li ZHAO (✉)[2], Weizhong ZHANG[3], Jiyan LI[4], Ruixiang ZHANG[1], Jianlei YANG[1], Guangzeng WANG[5]

1 Shandong Institute of Petroleum and Chemical Technology, Dongying 257061, China
2 College of Resources and Environment, Shandong Agriculture University, Tai'an 271018, China
3 Geophysical Research Institute of Shengli Oilfield Branch Company, SINOPEC, Dongying 257022, China
4 Research Institute of Petroleum Exploration & Development, Shengli Oilfield Company, SINOPEC, Dongying 257000, China
5 College of Marine Geosciences, Ocean University of China, Qingdao 266100, China

Abstract Hydrocarbon exploration in the Dongying Sag is constrained by the development of many Cenozoic transtensional structures with complex patterns and dynamic mechanisms. This study uses seismic interpretation and analog modeling to investigate these transtensional structures. Significant results include dividing these transtensional structures into boundary fault, oblique rifting, and deep strike-slip fault controlled structures, according to the relationships between main and secondary faults. They developed in the steep slope zone, the central sag zone, and the slope zone, respectively. In profile, the transtensional structures formed appear to be semi-flower-like, step-like, or negative-flower-like. In plan-view, they appear to be broom-like, soft-linked, or en-echelon structures. Further, these transtensional structures are controlled by the oblique normal slip of boundary faults, by the oblique extension of sub-sags, and by the later extension of deep strike-slip faults. The geometric deformation of these transtensional structures is controlled by the angles between the regional extension direction and the strike of boundary faults, deep faults, or sub-sags, where a larger angle corresponds to less developed transtensional structures. Further, the transtensional structures in the Dongying Sag were created by multi-phase and multi-directional extensions in the Cenozoic—which is also controlled by pre-existing structures. The strike of newborn secondary faults was determined by the regional extension direction and pre-existing structures.

Keywords transtensional structure, seismic interpretation, analogue modeling, dynamic mechanism, Dongying Sag

Received August 30, 2022; accepted November 29, 2022

E-mail: orchidy@126.com

1 Introduction

Transtensional structures describe extensional deformation with a component of strike-slip faulting, and is typically recognizable by en-echelon faults in plan-view (Harding, 1990; Yan and Wang, 1996). These structures form in strike-slip regimes with non-coaxial deformation (Dewey et al., 1998), as well as in extensional regimes with coaxial deformation (Keep and McClay, 1997; Morley et al., 2004; Mortimer et al., 2007). The latter typically develop along oblique-slip faults that may produce local non-coaxial deformation, especially under a multi-phase oblique extension (Morley et al., 2004). The concept of transtensional structures was first proposed to highlight the local fault extensions identified during the study of deformation patterns of large strike-slip faults (Harland, 1971; Fitch, 1972; Mann et al., 1983). The scope of the studies related to transtensional structures was subsequently modified, and the focus moved from strike-slip faults to oblique-slip faults, which were boundary-controlled or main faults within basins. Their tectonic setting was also expanded to include the oblique extension of plate margins or interiors (McCoss, 1986; Dewey et al., 1998; Fossen and Tikoff, 1998). Multi-phase and multi-directional extensions tend to occur in a rifting basin when the strike of pre-existing structures is not perpendicular to the later extension direction. As a result, some faults that underwent multi-phase extension slipped obliquely in the later phase, from which

secondary faults in en-echelon patterns were derived. Alternatively, the strike of secondary faults in the overlying strata could have been controlled by pre-existing deep faults, which caused them to be distributed in an en-echelon pattern (Schlische et al., 2002; Morley, 2007; Pongwapee et al., 2019; Wang et al., 2021). Finally, pre-existing structures typically combine with later secondary faults to form transtensional structures. However, transtensional structures have different dynamic mechanisms from transtension, and are commonly developed in localized areas of a rifting basin whose extension direction underwent changes with time (Keep and McClay, 1997; Morley et al., 2004; Mortimer et al., 2007).

Pre-existing structures are important factor controlling the deformation of rifting basins and thus, have always been the focus of studies both, in China and abroad. Through three-dimensional mechanical analysis and physical or numerical simulation, scholars analyze multi-phase extension and pre-existing structures, and their control on the structural styles of rifting basins in Thailand (Morley et al., 2004; Pongwapee et al., 2019), the North Sea (Bell et al., 2014; Phillips et al., 2019; Osagiede et al., 2020), East Africa (Corti et al., 2007; Mortimer et al., 2007; Wang et al., 2021), and the South China Sea (Suo et al., 2022). These studies concluded that the strikes, dips, linkage, and geometric shapes of pre-existing faults are important factors controlling the later oblique extensional deformation. Tong et al. (2010) quantitatively analyzed pre-existing fault activity within the stress field to determine whether pre-existing faults were reactivated at later stages, and also their effects on newborn faults. The results of analog modeling also suggest that en-echelon faults developing from single or multi-phase oblique rifting are normal rather than strike-slip or oblique-slip (McClay and White, 1995; Keep and McClay, 1997). However, they only focus on basin-wide secondary and newborn faults, ignoring the oblique slip from deep or boundary faults in multi-phase deformation. Subsequent analog models of two-phase and multi-directional extension show that the reactivating faults slip obliquely at later stages, thus controlling the strike of newborn faults (Tron and Brun, 1991; Bonini et al., 1997; Clifton et al., 2000; Sun et al., 2010; Duffy et al., 2015; Henstra et al., 2019). Despite of the difficulties in identifying the strike-slip characteristics of faults in a rift basin, these studies indicate that pre-existing boundary faults or main faults slipped obliquely at a later stage and combined with secondary faults to produce transtensional structures. In addition, when the basin or rift orientation is oblique to its later extension direction, oblique rifting and transtensional structures would develop in the central depression (Keep and McClay, 1997; Mortimer et al., 2007; Wang et al., 2021).

Although multiple studies have assessed the controlling effects of pre-existing structures on newborn faults, few studies focus on the types and deformation patterns of transtensional structures created by multi-phase extension. The Bohai Bay Basin was subject to transtension in the Late Mesozoic because of Tanlu Fault Zone, and experienced multi-phase and multi-directional extensions in the Cenozoic (Zong et al., 1999; Zhang et al., 2019; Wang et al., 2020; Hu et al., 2022). Thus, many transtensional structures developed within the basin as an effect of multiple dynamic mechanisms such as pull-apart (Allen et al., 1997; Hou et al., 2001), rifting (Liu et al., 2004; Li et al., 2013; Liang et al., 2016), and extension with strike-slip (Ye et al., 1985; Qi and Yang, 2010). Few studies focus on the effect of oblique extension and pre-existing structures on transtensional structures. This paper uses seismic interpretation to study the Dongying Sag and develop geological models for transtensional structures. It also uses analog modeling, by conducting single-factor experiments, to analyze the control effects of the angle between the strike of pre-existing structures and the later extension direction on the transtensional structures, and investigates the relationship between experimental results and actual data in terms of geometric deformation. This focus of this study is to improve the current understanding of the zonation, classification and mechanisms of formation of transtensional structures in the Dongying Sag, which is significant for hydrocarbon exploration as well as for understanding the multiple phases of structural deformation and dynamics of the Bohai Bay Basin.

2 Geological setting

The Dongying Sag is a secondary structural unit of the Jiyang Depression in the south-eastern Bohai Bay Basin. It is adjacent to the Tanlu Fault to the east, next to the Binxian, Linfanjia, and Qingcheng uplifts to the west, and borders the Luxi Massif to the south and the Chenjiazhuang Uplift to the north (Fig. 1(a)). In plan-view, the Dongying Sag consist of the Boxing, Niuzhuang, Lijin, and Minfeng sub-sags and several second-order structural zones. In profile-view, the Dongying Sag is faulted in the north and overlapped in the south. It has typical half-graben characteristics, and can be divided into a steep slope zone, a central sag zone, and a slope zone (Fig. 1(b)). The Dongying Sag is approximately 90 km long from east to west, and approximately 65 km wide from north to south. It hosts the richest hydrocarbon resources in the Jiyang Depression.

Three sets of faults occur in the Dongying Sag, striking NW–SE, nearly E–W, and NE–SW (Yi and Hou, 2002; Zheng et al., 2005; Zhang et al., 2006). The first set includes the Shicun Fault and the eastern segment of the Chennan Fault. The second set includes the middle segment of the Chennan Fault and the Shengbei Fault. The third set includes the western segment of the

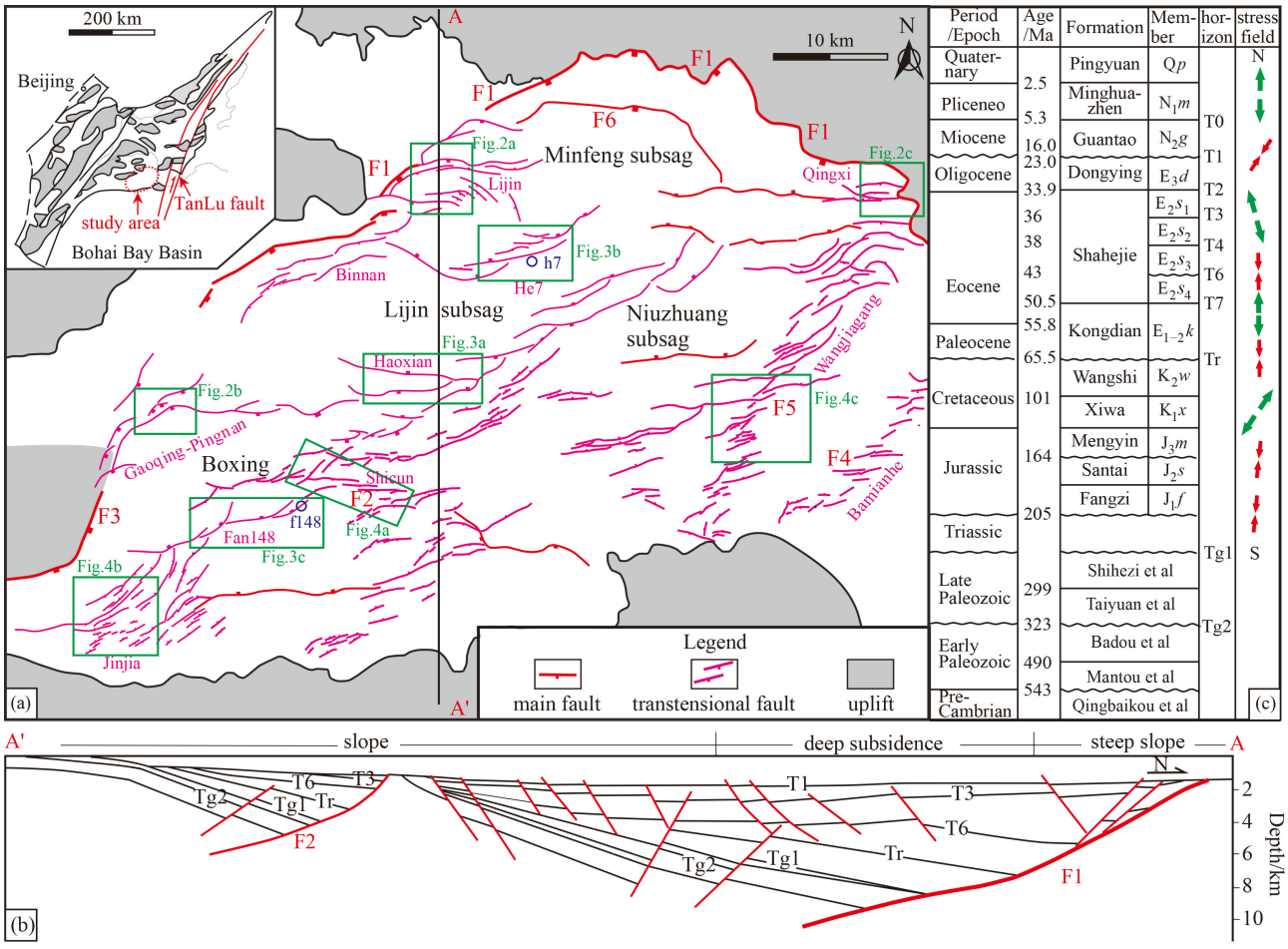

Fig. 1 Planimetric distribution of transtensional structures in seismic reflection of T2 (a), the stratigraphic column (b) and the structural profile of the Dongying Sag (c). Fault abbreviations used are F1–Chennan, F2–Shicun, F3–Gaoqing–Pingnan, F4–Bamianhe, F5–Wangjiagang, F6–Shengbei.

Chennan Fault, the Haoxian and Bamianhe faults, and the middle segment of the Gaoqing–Pingnan Fault. These three sets of faults were formed by the strike-slip movement of the Tanlu Fault between the Late Jurassic and the Early Cretaceous, the regional S–N extension in the Early Cenozoic, and NNW–SSE extension in the Late Cenozoic, respectively (Zong et al., 1999; Wu et al., 2003; Ren et al., 2009; Zhao and Li, 2016). It indicates that the extension direction of the Dongying Sag has rotated counterclockwise since the Late Mesozoic. Multi-phase faults and transtensional structures developed in the Dongying Sag under this tectonic setting.

The Dongying Sag has a similar sedimentary and structural evolution to the Jiyang Depression and the Bohai Bay Basin. It began as a Paleozoic cratonic basin, and underwent pre-rifting in the Mesozoic, Paleogene syn-rifting, and then post-rifting in the Neogene and Quaternary. Paleozoic rocks include the marine strata of the Cambrian–Ordovician and the alternate marine-continental strata of the Carboniferous–Permian. The Mesozoic strata are missing Triassic age rocks. The Lower and Middle Jurassic Fangzi and Santai formations consist of coal-bearing clastics. The Upper Jurassic and Cretaceous Mengyin, Xiwa, and Wangshi formations comprise fluvial-lacustrine clastics and volcanic sedimentary rocks. The Paleogene Kongdian ($E_{1-2}k$), Shahejie (E_2s), and Dongying (E_3d) formations consist of lacustrine clastics. The Neogene Guantao (N_1g) and Minghuazhen (N_2m) formations comprise lacustrine clastics. The Quaternary Pingyuan Formation (Qp) consists of clastics and unconsolidated loess. Of these, the Shahejie Formation is further divided into four members (E_2s_1, E_2s_2, E_2s_3, and E_2s_4, respectively). Further, reflection interfaces such as T1, T2, T7, Tr, and Tg1 can be identified in seismic profiles (Fig. 1(c)).

3 Classification and characteristics of transtensional structures

Transtensional structures such as Gaoqing–Pingnan, Jinjia, Bamianhe, Qingxi, Binnan–Lijin, Shicun, and Haoxian have been identified in the Dongying Sag based on seismic interpretation and analyses of the planar distribution of faults. Based on the relationship between the main and secondary faults and their structural

evolution, the transtensional structures in the Dongying Sag can be divided into three types of fault controlled structures — boundary fault, oblique rifting, and deep strike-slip fault controlled structures.

3.1 Boundary fault controlled transtensional structures

When a boundary fault controlling the sag or subsags undergoes multi-phase extension, its hanging wall would develop transtensional structures. Examples include the Binnan–Lijin, Gaoqing–Pingnan, and Qingxi (Fig. 1). Their boundary faults were developed in the steep slope zone of Dongying Sag, such as the western segment of the Chennan Fault, the Gaoqing–Pingnan Fault, and the eastern segment of the Chennan Fault, respectively. In plan-view, these secondary faults and boundary faults intersect obliquely and are combined into broom-like or inverted-broom-like structures (Fig. 2). In seismic profiles, the secondary faults end at the boundary faults and combine into semi-flower structures. Fault activity analysis suggests that secondary faults formed mainly in E_2s_3–E_3d. The direction of extension in the Dongying Sag were 50NE° in $E_{1\text{-}2}k$, S–N in E_2s_4, 330NW° in E_2s_3, 340NW° in E_2s_2, S–N in E_2s_1, 10NE° in E_3d according to balanced sections and derived paleostress information (Zhao, 2007). Contrastive analysis shows that the angle (30°−60°) between the strike of Gaoqing–Pingnan Fault and the regional extension direction in E_2s_3–E_3d was smaller than that of the western segment of the Chennan Fault (50°−80°) (Figs. 2(a) and 2(b)). As a result, the 50° angle between the strike of the secondary faults and Gaoqing–Pingnan Fault is larger than that of the western segment of the Chennan Fault (40°), and the broom-like structure is roughly in the shape of an ‘F’. The eastern segment of the Chennan Fault has a N–NW strike, creating an inverted-broom-like structure (Fig. 2(c)).

3.2 Oblique rifting controlled transtensional structures

Transtensional structures are produced when the later extension direction is not perpendicular to the rift strike, and the basins or depressions develop by oblique rifting (McClay and White, 1995; Brune et al., 2018; Basilone, 2022). The Dongying Sag, with NW–SE strike in the Late

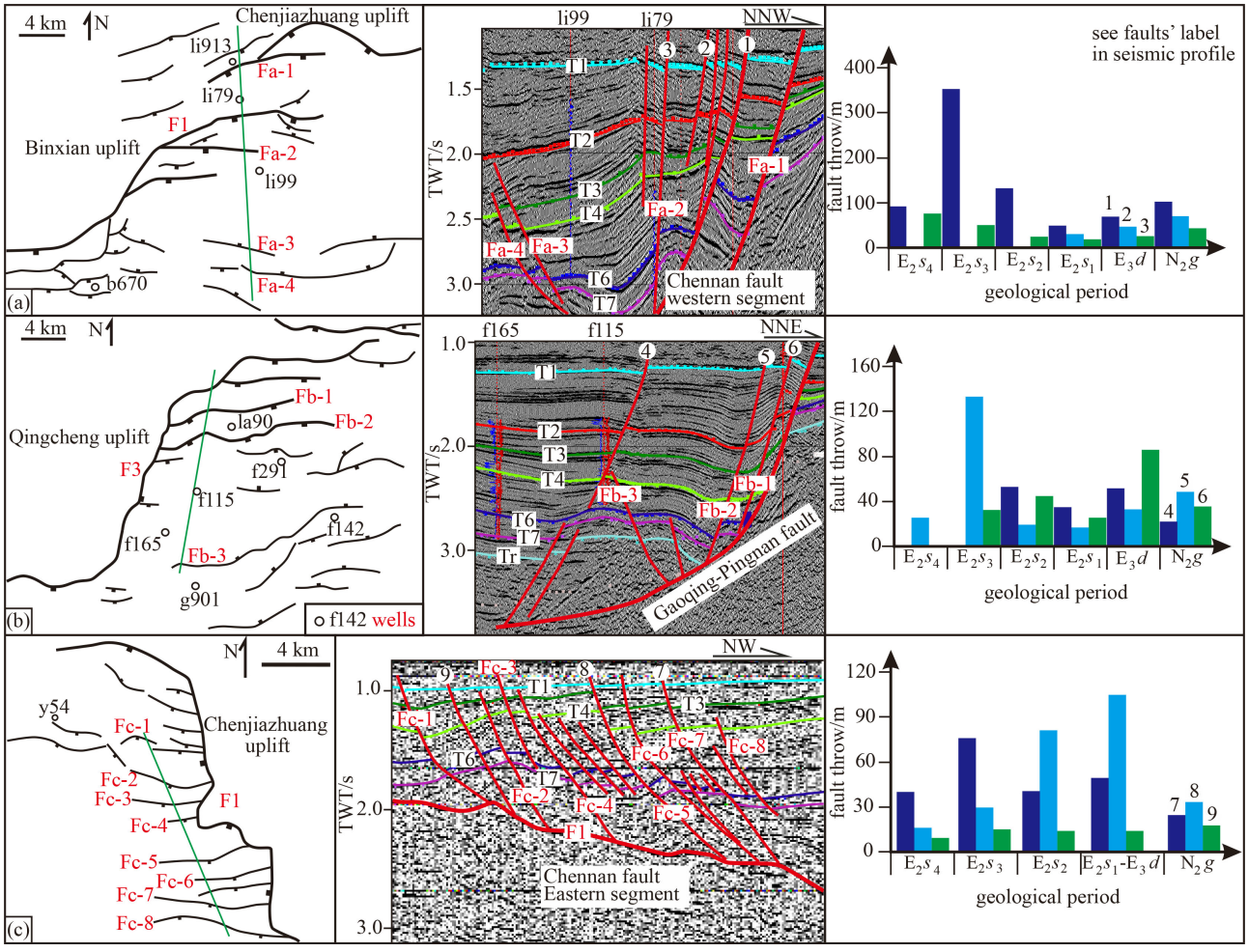

Fig. 2 Deformation characteristics of the Binnan–Lijin (a), Gaoqing–Pingnan (b), and Qingxi (c) transtensional structures. All faults appear in seismic reflection layer T6. Fault labels, seismic reflection interfaces, and location are the same as in Fig. 1.

Mesozoic, mainly underwent S–N and NW–SE regional extension in the Cenzonic. Transtensional structures, such as Haoxian, He-7 and Fan-148, developed in the Lijin and Boxing sub-sags, which are within the central sag zone of Dongying Sag (Fig. 1). In plan-view, these transtensional structures have no main fault, but are composed of a series of secondary faults. These faults are soft-linked and combine into an en-echelon pattern (Fig. 3). In seismic profiles, the faults are combined in a step pattern and exhibit a northward inclination. Fault activity analysis shows that these faults mainly developed in E_2s_3–E_3d. The Lijin and Boxing sub-sags were formed in $E_{1\text{-}2}k$–E_2s_4, with NE60° and NW280° strikes, respectively (Zhao and Li, 2016). These sub-sags were obliquely rifted when the regional extension direction was approximate NNW, and produced transtensional structures. The angle (60°−90°) between the strike of the Lijin sub-sag and the extension direction is bigger than that of the Boxing sub-sag (50°−80°). As a result, the faults of the transtensional structures in the Lijin sub-sag feature a higher degree of soft linkage and more significant transtensional deformation.

3.3 Deep strike-slip fault-controlled transtensional structures

The Jinjia, Wangjiagang, Bamianhe, and Shicun structures in the slope zone of the Dongying Sag host buried strike-slip faults (Fig. 1). Their reactivation in a later extension produced transtensional structures in the overlying strata on both sides. These deep strike-slip faults were produced by the strike-slip movements of the Tan–Lu Fault in the Late Jurassic and the Early Cretaceous, and they are widely distributed in the southern slope of the Jiyang Depression (Ren et al., 2009; Zhao and Li, 2017). These strike-slip faults extend from the north of the Luxi Massif toward the basin. In plan-view, the transtensional structures are composed of a series of R shears and T fractures in an en-echelon pattern (Fig. 4). In seismic profiles, the faults combine and appear as negative flower structures, whose floral axes consist of the (pre-Cenozoic) main fault in the deep and petals consist of the (Cenozoic) secondary faults in overlying strata. Differently from the Riedel shear style, the T fractures are far away from the deep faults and distributed on both sides. It indicates that these transtensional structures were created by the Cenozoic extension.

Fault activity analysis shows that the deep faults were predominantly active in the Mesozoic, while the secondary faults were active mainly in $E_{1\text{-}2}k$–E_2s_4, with some activity persisting until E_3d. The Dongying Sag was a zone of extensional deformation in the Cenozoic. In

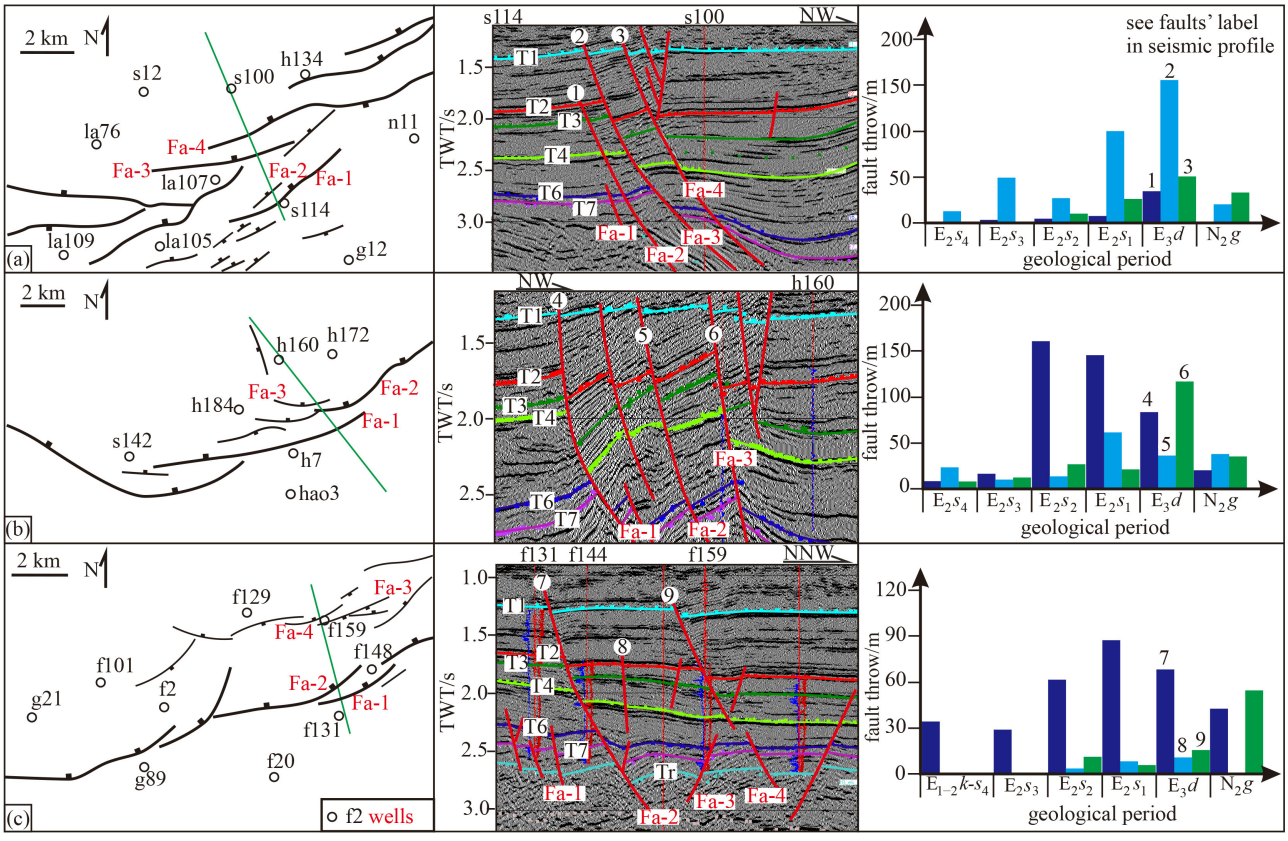

Fig. 3 Deformation characteristics of the Haoxian (a), He-7 (b) and Fan-148 (c) transtensional structures. All faults appear in the seismic reflection layer T6. Seismic reflection interfaces and location are the same as in Fig. 1.

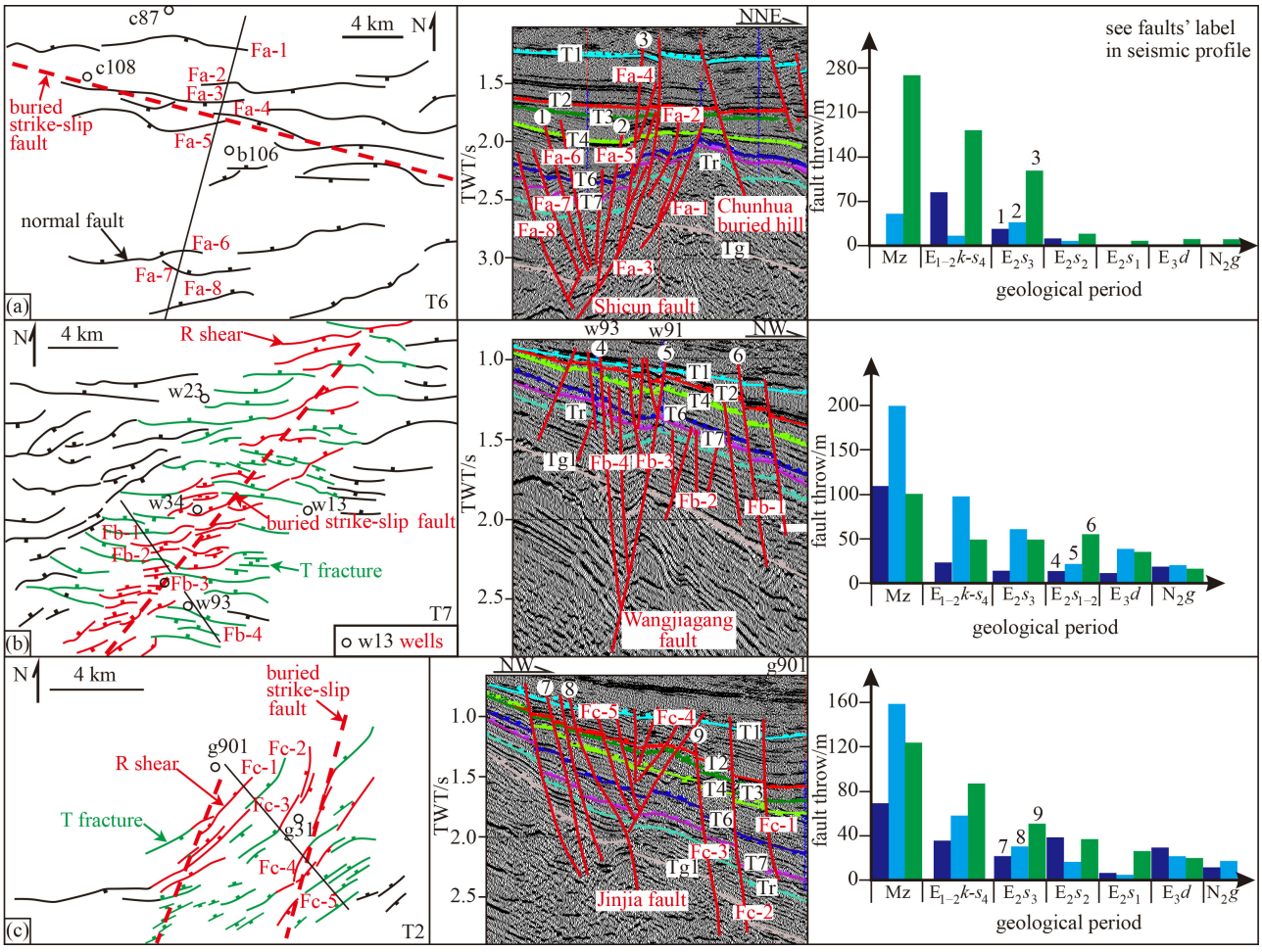

Fig. 4 Deformation characteristics of the Shicun (a), Wangjiagang (b) and Jinjia (c) transtensional structures. The faults are distributed in seismic reflection layers T6, T7, and T2. Seismic reflection interfaces and location are the same as in Fig. 1.

comparison, the Shicun Fault has the largest angle (50°−80°) between its strike and regional extension direction in the Cenozoic, and its secondary faults follow a mainly normal pattern. This indicates that the Shicun Fault was an extensional structure in the Cenozoic (Fig. 4(a)). The Wangjiagang and Bamianhe faults are second to the Shicun Fault in terms of the fault angles to the regional extension direction (30°−60°, 40°−70°). Their secondary faults, which developed in the Cenozoic, include R shears and T fractures. This indicates an equal control from both, strike-slip and extensional deformation during their formation (Fig. 4(b)). The Jinjia Fault has the smallest angle with the regional extension direction (20°−50°), where a strike-slip fault zone composed of R shears developed in the Cenozoic, indicating that the evolution of the Jinjia structure was influenced by strike-slip movement (Fig. 4(c)).

4 Analogue modeling

Comparisons of the different transtensional structures show that the angle between the varying extension direction and the pre-existing structures significantly affected the subsequent activity of pre-existing faults, as well as the strike and nature of newborn secondary faults. Analogue modeling was conducted as follows.

4.1 Materials and scaling

Experiments were conducted at the Deep and Tight Hydrocarbon Laboratory of the Shandong Institute of Petroleum and Chemical Technology using a structural physical simulator and a 3D terrain scanner. Experimental materials include 120-mesh quartz sands with cohesion of approximately 200 Pa, an internal friction angle of 30°, and a density of 1.8 g/cm^3. Quartz sands are commonly used to simulate the deformation of the upper crust, and their deformation conforms to the Mohr-Coulomb criterion.

Analogue modeling follows the similarity criterion between experimental and geological models in geometry, kinematics and dynamics. For brittle deformation, the related parameters of the experimental

and geological models should comply with the following formula (Weijermars and Schmeling, 1986):

$$\sigma^* = C^* = \rho^* \cdot g^* \cdot l^*, \quad (1)$$

where σ^*, C^*, ρ^*, g^*, and l^* are the similarity ratios of stress, cohesion, density, gravity and length between the experimental and geological models, respectively. For the experimental models in this study, sand bodies with a length of 1 cm were used to simulate strata with a thickness of 1–2 km, and these models had l^* of approximately $0.5–1.0 \times 10^{-5}$. The experiments were performed under natural gravity, with g^* of 1.0. In the Dongying Sag, Cenozoic strata are mainly composed of sandstones (ρ: ~2.6 g/cm^3) and mudstones (ρ: ~1.9 g/cm^3), which have ρ^* of approximately 0.69–0.95 as compared with quartz sands. The C^* was calculated to be about $3.5–9.5 \times 10^{-6}$ using the similarity formula, and the cohesion of rocks in the geological models was approximately 21–57 MPa, conforming to the experimental principle and the geophysical parameters of natural rock (Schellart, 2000).

4.2 Design

This study designed nine groups of single-factor experiments for the three types of transtensional structures (Table 1). Models M1, M2, and M3 were designed to represent boundary fault controlled transtensional structures. Foam boards were arranged in the northern portion to simulate uplifts and pre-existing boundary faults, such as Chenjiazhuang Uplift and Chennan Fault (Fig. 2(c)). The angles between the strike of the foam boards and the extension direction were set at 22.5°, 45°, and 67.5° (Fig. 5(a)). The M1 model approximately simulates the Gaoqing–Pingnan transtensional structures for NNW-SSE regional extension in E_2s_3–E_3d. The M2 model simulates the Lijin transtensional structures for S–N regional extension in $E_{1\text{-}2}k$–E_2s_4. The M3 model simulates the Qingxi transtensional structures for S–N regional extension in $E_{1\text{-}2}k$–E_2s_4.

Models M4, M5, and M6 were designed to produce oblique rifting controlled transtensional structures for which foam boards were symmetrically arranged in the northern and southern portions to simulate uplifts or buried hills, such as Binxian Uplift and Chunhua buried hills (Fig. 1). The angles between the strike of the foam boards and the extension direction were set at 30°, 45°, and 60° (Fig. 5(b)), approximately simulating the Fan-148, Haoxian and He-7 transtensional structures for NNW–SSE regional extension in E_2s_3–E_3d.

Models M7, M8, and M9 were designed to represent deep strike-slip fault controlled transtensional structures. The rubber sheets at the bottom were cut into two parts to simulate deep strike-slip faults, e.g., the Wangjiagang Fault in Fig. 4(b). The angles between the strike of the cutting line in the rubber sheets and the extension direction were set at 22.5°, 45°, and 67.5° (Fig. 5(c)). The M7 model approximately simulates the Jinjia transtensional structures for NNW–SSE regional extension in E_2s_3–E_3d. The M8 model simulates Bamianhe and Wangjiagang transtensional structures for S–N regional extension in $E_{1\text{-}2}k$–E_2s_4. The M9 model simulates the Shicun transtensional structures for S–N regional extension in $E_{1\text{-}2}k$–E_2s_4.

The rubber sheet at the bottom of the sand bodies was extended southward at a speed of 0.02 mm/s for models M1, M2, and M3. The rubber sheet was extended southward and northward at speeds of 0.008 mm/s and 0.005 mm/s for models M4, M5, and M6, and at 0.012 mm/s and 0.008 mm/s for models M7, M8, and M9. These nine groups of experiments lasted for 42–45 min. Each of the sand bodies had a thickness of 4 cm, width of 30 cm, and a length of 45 cm (Fig. 5(d)). They were extended for 5.0–5.4 cm.

Table 1 Experimental design of transtensional structures

Types	Geological models	Experiments			
		Models	Angles	Time	Speed
Boundary fault controlled	Gaoqing-Pingnan in E_2s_3-E_3d	M1	22.5°	45 min	v_s = 0.02 mm/s
	Lijin in $E_{1\text{-}2}k$-E_2s_4	M2	45°		
	Qingxi in $E_{1\text{-}2}k$-E_2s_4	M3	67.5°		
Oblique rifting controlled	Fan-148 in E_2s_3-E_3d	M4	30°	42 min	v_s = 0.008 mm/s v_n = 0.005 mm/s
	Haoxian in E_2s_3-E_3d	M5	45°	42 min	
	He-7 in E_2s_3-E_3d	M6	60°	42 min	
Deep strike-slip fault controlled	Jinjia in E_2s_3-E_3d	M7	22.5°	43 min	v_s = 0.012 mm/s v_n = 0.008 mm/s
	Bamianhe, Wangjiagang in $E_{1\text{-}2}k$-E_2s_4	M8	45°	43 min	
	Shicun in $E_{1\text{-}2}k$-E_2s_4	M9	67.5°	43 min	

Notes: Angles refers to the angle between the extension direction and the strike of the foam boards or the cutting line on the rubber sheet.v_s, v_n refers to the speed of rubber sheets extended southward and northward.

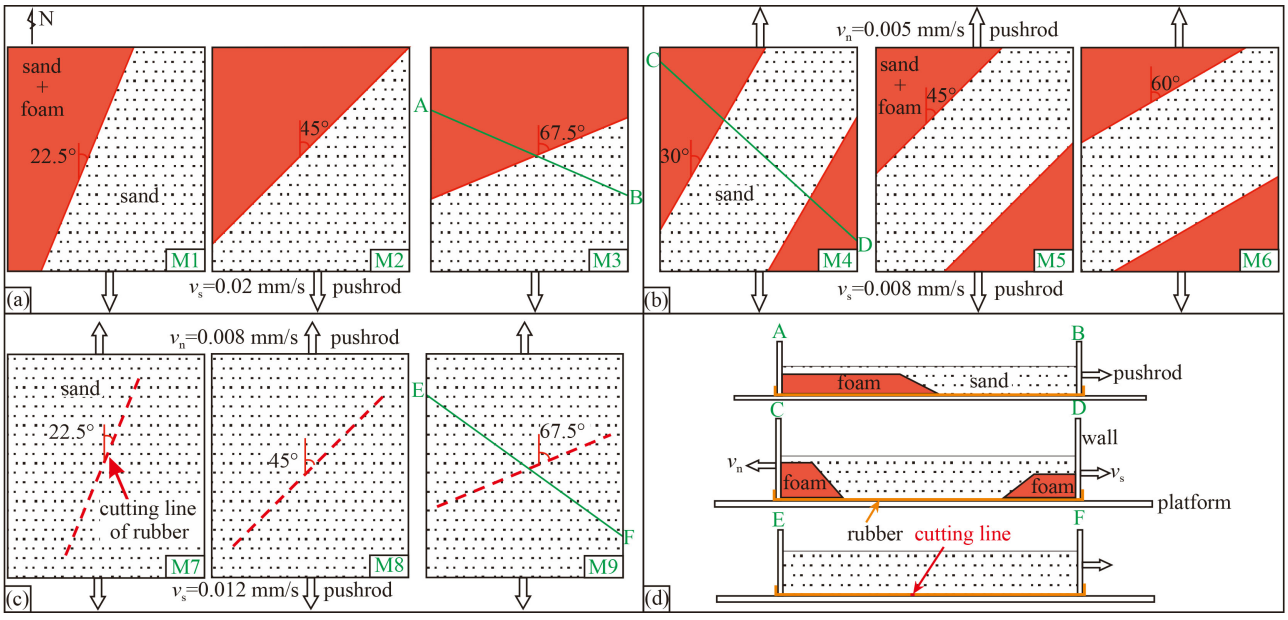

Fig. 5 Experimental models designed for boundary fault (a), oblique rifting (b), and deep strike-slip (c) controlled transtensional structures. Figure sub-parts are in plan-view and profile view (d) of the experimental models.

4.3 Experimental results

The elevation of the sand body surface was obtained using the 3D terrain scanner at a 1-min interval to record the deformation process of the sand bodies. After the experiment, the 3D digital elevation data were plotted and interpreted as follows.

In the M1 model, the boundary faults mainly underwent strike-slip deformation, and NE–SW and nearly E–W secondary faults developed in the sand body (Fig. 6(a)). The NE–SW secondary faults were close to the boundary fault, and the two were hard linked. As a result, the boundary fault significantly affected the strike of the secondary faults, which were not perpendicular to the extension direction. They distributed in a planar en-echelon pattern, and combined into a broom shape with the boundary fault. The nearly E–W secondary faults were far away from the boundary faults and perpendicular to the extension direction. In the M2 model, the boundary faults showed weaker strike-slip deformation. The sand body developed NE–SW and NWW–SEE secondary faults in the northern and southern, respectively (Fig. 6(b)). The northern secondary faults and the boundary fault combined into a broom shape because of the same mechanics with NE–SW secondary faults in the M1 model. However, the rubber sheet extended southward at a higher speed, and the southern boundary fault extended more intensively than the northern. As a result, the NWW–SEE secondary faults were more inclined to be perpendicular to the extension direction than NE–SW secondary faults. In the M3 model, the boundary faults were dominated by extension and combined with the secondary faults into a broom shape (Fig. 6(c)). As the angle between the main fault strike and the extension direction increased, the effect of the main fault on the secondary faults strike weakened. The NWW and NEE secondary faults were conjugate and nearly perpendicular to the extension direction. This model exhibited a large angle between the secondary faults strike and the extension direction, indicating that the sand body mainly underwent the extension.

In the M4 model, the boundary faults were formed first and were dominated by strike-slip deformation (Fig. 6(d)). The secondary faults in the sand body intersected with the boundary faults and had a strike close to E–W. In the M5 model, the boundary faults developed weak strike-slip movements, and were tangent to the secondary faults in the sand body. They combined into broom and inverted-broom shapes, and the NEE–SWW secondary faults distributed contemporaneously in an en-echelon pattern (Fig. 6(e)). In the M6 model, the boundary faults and the secondary faults in the sand body were dominated by extension (Fig. 6(f)). The NEE–SWW and NWW–SEE secondary faults developed in the southern and northern regions, respectively. Higher extension speeds ensured the southern secondary faults were more intensely affected by the boundary fault as compared to those in the north. As a result, the former secondary faults were parallel to the southern boundary fault. The later were slightly oblique to the northern boundary fault, and combined the boundary faults into a broom shape.

In the M7 model, R shears and T fractures developed in the sand bodies above the deep faults and evolved into the primary deformation zone (PDZ), showing significant strike-slip characteristics (Fig. 6(g)). Nearly E–W oriented normal faults developed in both walls of the

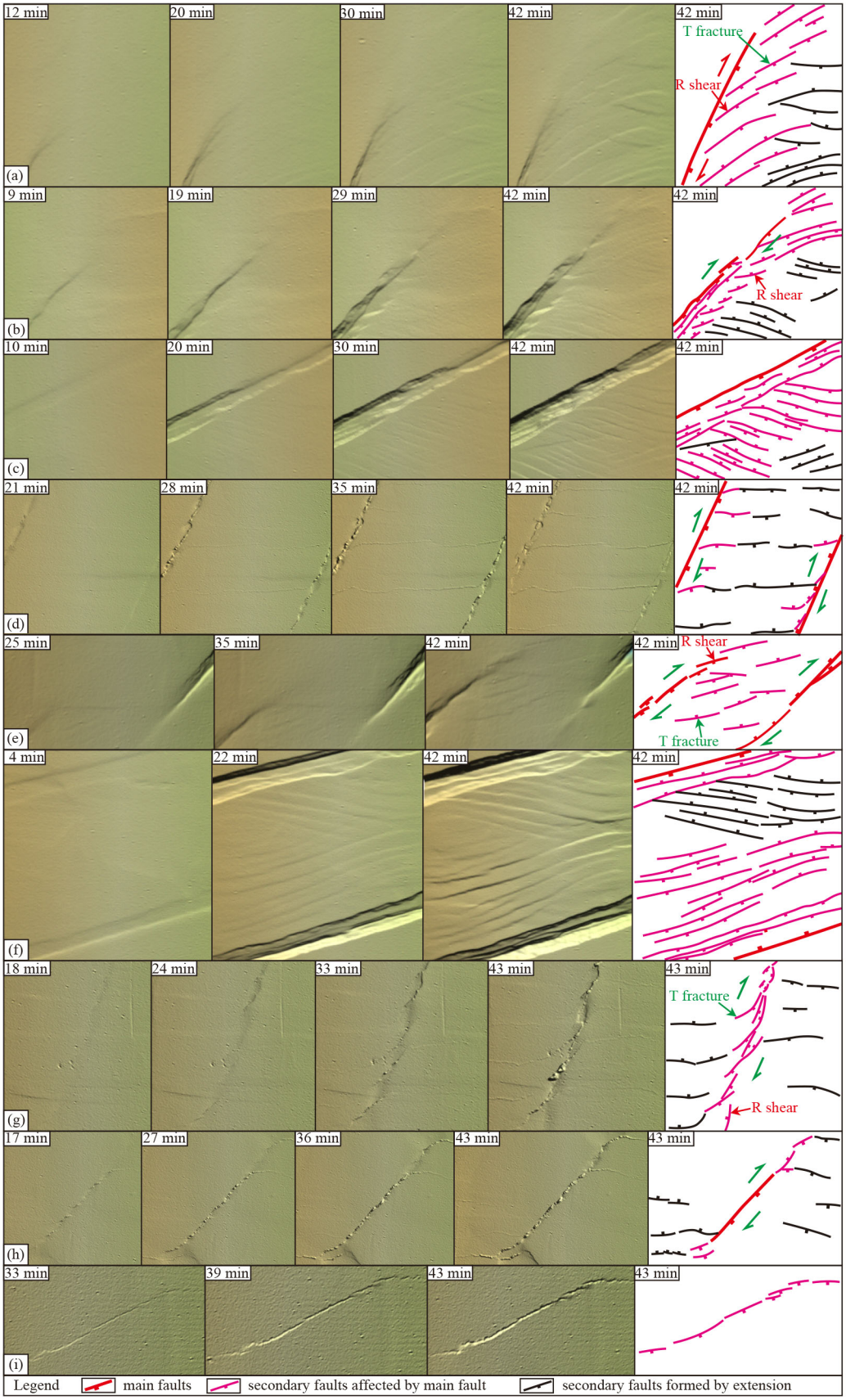

Fig. 6 Experimental results and their interpretations for models M1 (a), M2 (b), M3 (c), M4 (d), M5 (e), M6 (f), M7 (g), M8 (h), M9 (i).

deep strike-slip fault, and distributed in a planar pattern. These faults and the PDZ combined into transtensional structures, which were different from the Riedel shear deformation. In the M8 model, small en-echelon faults developed above the deep faults, and finally expanded into the PDZ (Fig. 6(h)). Meanwhile, NWW–SEE normal faults developed in both walls of the deep strike-slip fault. In the M9 model, multiple en-echelon faults evolved into one fault, forming an overall 'S' shape (Fig. 6(i)). The sand body in this model mainly underwent extension, and almost no secondary faults were developed.

4.4 Relationship between the models and actual data

The experimental results of the M1, M2, and M3 models compare well with actual data, suggesting that the sand bodies experienced similar deformations. They exhibit broom-like structures planarly and semi-flower-like structures in profiles. The differences among them are related to the increasing angle between the boundary fault strike and the extension direction where the extension of the boundary faults intensified while the strike-slip movement weakened. The intersection angles between the secondary and boundary faults gradually increased. These angles were 28° in M1, 35° in M2, and 52° in M3 (Figs. 6(a), 6(b), 6(c)), which respectively correspond with the angles between Gaoqing–Pingnan (30°), Lijin (34°), and the Qingxi (59°) transtensional structures and their main faults (Fig. 2). This suggests that a corresponding relationship exists between the geological and experimental models in terms of their geometric deformation.

In the M4, M5, and M6 models, their secondary faults were all connected by soft linkage, distributed in an en-echelon pattern, and they combine with the boundary faults into a broom-like structure. In contrast with the previous models, as the angle between the strike of the sand bodies and the extension direction increased, the dominant deformation of the boundary faults changed from strike-slip to extension, and the deformation of the secondary faults in the sand bodies intensified. The style of the boundary faults, when combined with the secondary faults, transitioned from broom-like to parallel patterns. And the angles between the secondary faults strike and sandbodies orientation gradually decreased. That angles were 53° in M4, 30° in M5, and almost 0° in M6 (Figs. 6(d), 6(e), 6(f)), which respectively correspond to the angles between Fan-148 (40°), Haoxian (21°) and He-7 (8°) transtensional structures and their sub-sags (Fig. 3).

In the M7, M8, and M9 models, the PDZ is developed by deep strike-slip faults that drive the overlying sand bodies to deform continuously. Here, as the angle between the extension direction and the strike of deep faults increased, the strike-slip of the PDZ in the overlying sand bodies weakened, while the extension intensified. The overall deformation of the sand bodies weakened, indicating the deep strike-slip faults not as active in the later stage. The geometric deformation in the M7 model is similar to the Jinjia transtensional structures (Fig. 4), as is the relationship between the M8 model and Bamianhe and Wangjiagang faults, and between the M9 model and the Shicun transtensional structure.

The comparison of the experimental results of these models (from M1 to M9) indicate that the strikes of newborn secondary faults are not perpendicular to the extension direction, and are significantly controlled by the pre-existing structures. As shown in the experiments, the angle between the strike of the secondary faults and their extension directions ranged between 51°–74°, 68°–72°, 67°–76°, 78°–87°, 76°–78°, 45°–70°, 83°–88°, 80°–87°, and almost 90°, respectively. It suggests that the strike of the secondary faults is strongly controlled by the boundary faults and less strongly by the deep strike-slip faults. This could be attributed, in part, to the development of deep strike-slip faults in a slope zone some distance away from the intensive deformation area, which was reactivated weakly. It also suggests that the structural deformation of deep strike-slip faults is concentrated mainly in the PDZ, while that of boundary faults is evenly distributed on the hanging walls. As a result, the strike of secondary faults is more inclined to be perpendicular to the regional extension direction in the M7, M8 and M9 models.

The strike of the secondary faults results from a combination of the regional extension direction as well as the strike and nature of pre-existing structures. Thus, the strike of newborn secondary faults can qualitatively, if not quantitatively, suggest the regional extension direction. Three-dimensional mechanical analysis, for example, using physical and numerical modeling can effectively resolve this problem. Previous studies analyzed the Cenozoic extension direction of the Dongying Sag using rose diagrams of the strike of secondary faults or their balanced sections. They concluded that the Dongying Sag had an extension direction of NW–SE in Es_3–Ed (Zhao, 2007; Zhan et al., 2012; Wu et al., 2015). However, these methods are based only on the strike of secondary faults or normal faulting, and do not consider the effects of pre-existing structures and strike-slip deformation. This renders their conclusion unreasonable. The experimental results from this study suggest that the Dongying Sag should have had an extension direction of NNW–SSE in Es_3–Ed.

5 Discussion on dynamic mechanisms

5.1 Pre-rift: compression in the Late Triassic

In the Early and Middle Triassic, the Bohai Bay Basin

was a large intracontinental basin with no significant active faulting (Qi et al., 2003; Wu et al., 2007; Li et al., 2012). In the Late Triassic, structural deformation in the south-east North China Craton was controlled by the subduction of the Yangtze Plate, and it underwent a change in compression direction from SSW to NNE (Wu et al., 2003; Ren et al., 2009; Li et al., 2017). As a result, nearly E–W folds and arcuate faults formed in the Jiyang Depression, which includes the Chennan Fault (Wu et al., 2003; Ren et al., 2009; Fig. 7(a)). Differential compression was adjusted by nearly S–N secondary strike-slip faults (Zhao and Li, 2017). In the Early and Middle Jurassic, the study area inherited the former structural deformation but the stresses were considerably weakened, as is characterized by denuded uplifts and filled sags (Wu et al., 2003). Overall, the Early Mesozoic regional compression and the formation of reverse faults constituted the first phase of pre-existing structural development in the study area.

5.2 Pre-rift: Transtension in the Late Jurassic and Early Cretaceous

In the Late Jurassic and Early Cretaceous, the Izanagi Plate subducted beneath the Eurasian Plate, which produced a NW–SE regional compression (Maruyama et al., 1997). Contemporaneously, the Tanlu Fault underwent intense sinistral strike-slip movement (Zhu et al., 2003, 2018). Under these tectonic settings, transtension and rifting depressions developed in the eastern Bohai Bay Basin and the Luxi Massif area (Zhu et al., 2018). As a result, the eastern segment of the NW–SE Chennan Fault and the NWW–SSE Shicun Fault in the Dongying Sag underwent negative inversion and transtensional deformation (Fig. 7(b)). These strike-slip faults are distributed in an en-echelon pattern, in combination with the Luoxi and Guxi faults to the north of the Dongying Sag. They have been modeled as transtensional structures in a sag or depression (Wu et al., 2003, 2007; Zhu et al., 2018). Strike-slip faults such as the Jinjia, Bamianhe, and Wangjiagang structures formed in the slope zone (Ren et al., 2009; Fig. 7(b)). In the Late Cretaceous, the eastern North China plate was uplifted and eroded, and red fluvial and lacustrine clastics were locally deposited in the study area (Wu et al., 2007). In the Late Mesozoic, the eastern segment of the Chennan Fault, the Shicun Fault, and other strike-slip faults in the slope zone constituted the second phase of development of pre-existing structures in the study area.

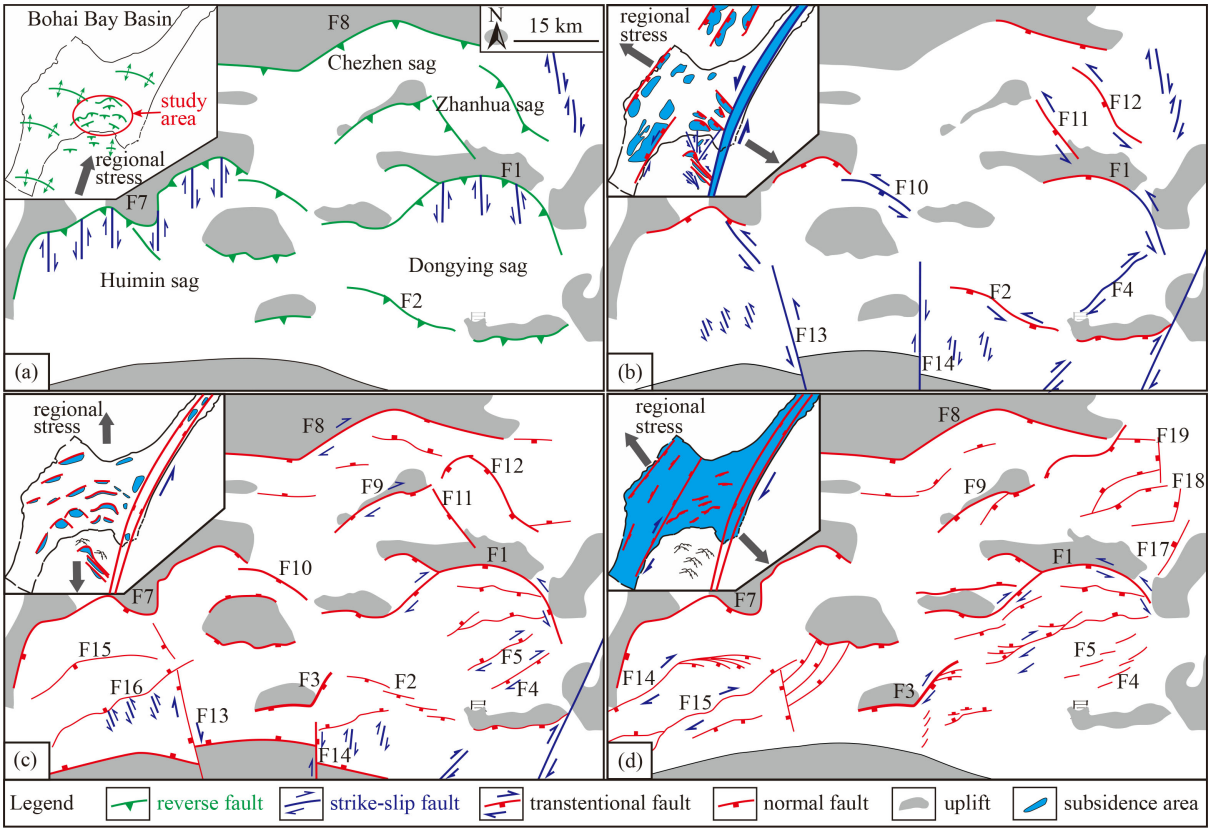

Fig. 7 The tectonic settings of transtensional structures in the Jiyang Depression with an inset map showing the position of the Jiyang Depression within the Bohai Bay Basin, and the regional stress direction during the (a) Indosinian, (b) Late Jurassic – Early Cretaceous, (c) $E_{1\text{-}2}k$–E_2s_4 and (d) E_2s_3–E_3d tectonic periods. Fault abbreviations used are F7–Ningwu, F8–Chengnan, F9–Yinan, F10–Zizhen, F11–Luoxi, F12–Guxi, F13–Baiqiao, F14–Cicun, F15–Linyi, F16–Xiakou, F17–Kendong, F18–Gudong, F19–Changdi.

5.3 Syn-rift: S–N extension in the Paleocene and Early Eocene

In $E_{1\text{-}2}k$–E_2s_4, the effect of slab window caused the asthenosphere mantle to upwell and exerted a S–N extension on the lithosphere (Thorkelson, 1996; Wu and Wu, 2019). The Tan–Lu fault experienced weak sinistral strike-slip motion and thus, had slight effects on the study area and the area to the west of the fault (Zhao and Li, 2016). Under these tectonic settings, a S–N regional extension developed in the study area and its adjacent areas (Wang et al., 2022). As a result, the E–W oriented middle segment of the Chennan Fault and the Shengbei Fault were intensely re-activated (Wu et al., 2003; Zheng et al., 2005). The eastern segment of the Chennan Fault, the Shicun Fault, and the secondary strike-slip faults in the slope zone continued to be active (Zhao and Li, 2017). The NE–SW trending western segment of the Chennan Fault and the Gaoqing–Pingnan Fault began to develop (Zhang et al., 2006; Ren et al., 2009; Fig. 7(c)). In this period, the Shicun, Qingxi, Wangjiagang, Bamianhe, and Jinjia transtensional structures began to form, and underwent the first phase of oblique extension.

5.4 Syn-rift: NNW–SSE extension in the Late Eocene and Oligocene

In E_2s_3–E_3d, the subduction of the Pacific Plate beneath the Eurasian Plate as well as the remote effect of the Qinghai–Tibet Plateau uplift resulted in a NWW–SEE regional extension, and the upwelling mantle resulted in a NW–SE extension of the lithosphere (Maruyama et al., 1997; Zhong et al., 2001). The movement of Tanlu fault transformed from the sinistral strike-slip into dextral (Wang et al., 2022). As a result of these geological processes, the Bohai Bay Basin and its internal sags extended in a NNW–SSE direction, leading to enhanced activity of the NE–SW oriented western segment of the Chennan Fault and Gaoqing–Pingnan Fault. The Jinjia Fault and the middle segment of the Chennan Fault continued to develop, but the Shicun, Bamianhe, and the eastern segment of the Chennan faults gradually ceased their development (Fig. 7(d)). In this period, the former transtensional structures continued to develop, and underwent a second phase of oblique extension. The transtensional structures such as Gaoqing–Pingnan, Haoxian, Binnan–Lijin began to form.

5.5 Post-rift: subsidence in the Neogene and Quaternary

In the Neogene and Quaternary, the subduction of the Pacific Plate beneath the Eurasian Plate leads the rifting in east China to migrate from the Bohai Bay Basin to the East China Sea and the Sea of Japan (Suo et al., 2014; Zhao and Li, 2017). As a result, structural deformation of the Bohai Bay Basin ended except in Bohai Bay area. In this period, the study area entered a post-rift stage, where the faults and transtensional structures that formed in the early stage gradually became inactive. They were buried at a depth of about 1000 m in the Neogene and Quaternary.

6 Conclusions

1) The transtensional structures in the Dongying Sag can be divided into three types based on the relationship between the main and secondary faults and their structural evolutions namely boundary fault, oblique rifting, and deep strike-slip fault controlled structures. These structures developed in the steep slope zone, the central sag zone, and the slope zone of the sag, respectively. The boundary fault controlled transtensional structures appear broom-like in plan-view and as semi-flowers in profile, e.g. the Binnan–Gaoqing and Qingxi structures. The oblique rifting controlled transtensional structures appear to be laterally-soft-linked, and show en-echelon patterns in plan-view and step-like patterns in profile, like the Haoxian and Fan-148 structures. The deep strike-slip fault controlled transtensional structures show an en-echelon pattern in plan-view and negative flowers in profiles, like the Jinjia and Wangjiagang structures.

2) Structural analysis and analog modeling show that boundary fault-controlled transtensional structures formed by the oblique normal faulting of boundary faults; oblique extension of the sub-sags produced the oblique rifting-controlled ones; and the deep strike-slip fault controlled structures were created by the later extension of the deep strike-slip faults. The strike of newborn secondary faults resulted from the combination of the regional extension and pre-existing structures. The pattern of transtensional structures is mainly controlled by the angle between the regional extension direction and the strike of the boundary faults, deep faults, or sub-sags. A larger angle corresponds to less developed transtensional structures.

3) The transtensional structures in the Dongying Sag resulted from the multi-phase extensions in varying stress regimes that it underwent in the Cenozoic. Regional pre-existing structures include reverse faults and deep strike-slip faults formed by the regional S–N compression in the Late Triassic and subsequent transtension in the Late Jurassic and Early Cretaceous. In $E_{1\text{-}2}k$–E_2s_4, the S–N extension allowed for the initial development of boundary and deep strike-slip fault controlled transtensional structures. In E_2s_3–E_3d, the NNW–SSE extension furthered the development of the boundary and deep strike-slip fault controlled transtensional structures, and aided the formation of the oblique rifting controlled transtensional structures.

Acknowledgments The authors thank the anonymous reviewers and

editors for their constructive comments and corrections which helped improve the manuscript. Seismic data was provided by the Shengli Oil Company Ltd., Sinopec. Natural Science Foundation Project of Shandong Province (No. ZR2020MD036) and the This study was financially supported by the National Natural Science Foundation of China (Nos. 42072162 and 42072235).

Competing interests The authors declare that they have no competing interests.

References

Allen M B, Macdonald D I M, Xun Z, Vincent S J, Brouet-Menzies C (1997). Early Cenozoic two-phase extension and late Cenozoic thermal subsidence and inversion of the Bohai Basin, northern China. Mar Pet Geol, 14(7–8): 951–972

Basilone L (2022). Jurassic-Cretaceous intraplatform basins from NW Sicily fold and thrust belt: implications for oblique rifting of the Southern Tethyan margin. Sediment Geol, 440: 106255

Bell R E, Jackson C A L, Whipp P S, Clements B (2014). Strain migration during multiphase extension: observations from the northern North Sea. Tectonics, 33(10): 1936–1963

Bonini M, Souriot T, Boccaletti M, Brun J P (1997). Successive orthogonal and oblique extension episodes in a rift zone: laboratory experiments with application to the Ethiopian Rift. Tectonics, 16(2): 347–362

Brune S, Williams S E, Müller R D (2018). Oblique rifting: the rule, not the exception. Solid Earth, 9(5): 1187–1206

Clifton A E, Schlische R W, Withjack M O, Ackermann R V (2000). Influence of rift obliquity on fault-population systematics: results of experimental clay models. J Struct Geol, 22(10): 1491–1509

Corti G, van Wijk J, Cloetingh S, Morley C K (2007). Tectonic inheritance and continental rift architecture: numerical and analogue models of the East African Rift system. Tectonics, 26(6): TC6006

Dewey J F, Holdsworth R E, Strachan R A (1998). Transpression and transtension zones. In: Holdsworth R E, Strachan R A, Dewey J F, eds. Continental Transpressional and Transtensional Tectonics, Geological Society, London, Special Publication, 135: 1–14

Duffy O B, Bell R B, Jackson C A L, Gawthorpe R, Whipp P S (2015). Fault growth and interactions in a multiphase rift fault network: Horda Platform, Norwegian North Sea. J Struct Geol, 80: 99–119

Fitch T J (1972). Plate convergence, transcurrent faults, and internal deformation adjacent to southeast Asia and the western Pacific. J Geophys Res, 77(23): 4432–4460

Fossen H, Tikoff B (1998). Extended models of transpression and transtension, and application to tectonic settings. Spec Publ Geol Soc Lond, 135(1): 15–33

Harding T P (1990). Identification of wrench faults using subsurface structural data: criteria and pitfalls. AAPG Bull, 74(10): 1590–1609

Harland W B (1971). Tectonic transpression in caledonian spitsbergen. Geol Mag, 108(1): 27–41

Henstra G A, Berg Kristensen T, Rotevatn A, Gawthorpe R L (2019). How do preexisting normal faults influence rift geometry? A comparison of adjacent basins with contrasting underlying structure on the Lofoten Margin, Norway Basin Res, 31(6): 1083–1097

Hou G T, Qian X L, Cai D S (2001). The tectonic evolution of Bohai basin in Mesozoic and Cenozoic time. Acta Scientiarum Naturalium Universitatis Pekinensis, 37(6): 845–851 (in Chinese)

Hu P P, Yang F L, Zhang R C, Wang W, Dong R W (2022). Cenozoic extension to strike-slip transition in the Liaodong Bay Subbasin along the Tan-Lu Fault Zone, Bohai Bay Basin: new insights from stress field modeling. Tectonophysics, 822: 229163

Keep M, McClay K R (1997). Analogue modelling of multiphase rift systems. Tectonophysics, 273: 239–270

Li S Z, Suo Y H, Santosh M, Dai L M, Liu X, Yu S, Zhao S J, Jin C (2013). Mesozoic to Cenozoic intracontinental deformation and dynamics of the North China Craton. Geol J, 48(5): 543–560

Li S Z, Zhao G C, Dai L M, Liu X, Zhou L H, Santosh M, Suo Y H (2012). Mesozoic basins in eastern China and their bearing on the deconstruction of the North China Craton. J Asian Earth Sci, 47(30): 64–79

Li S Z, Zheng Q L, Li X Y, Zhao S J, Suo Y H, Guo L L, Wang Y M, Zhou Z Z, Liu X G, Lan H Y, Zhang J, Guo R H, Li S J (2017). Triassic subduction polarity and orogenic process of the Sulu orogen, east China. Ma Geo Quat Geo, 37(04): 18–32 (in Chinese)

Liang J T, Wang H L, Bai Y, Ji X Y, Duo X M (2016). Cenozoic tectonic evolution of the Bohai Bay Basin and its coupling relationship with Pacific Plate subduction. J Asian Earth Sci, 127: 257–266

Liu M, Cui X J, Liu F T (2004). Cenozoic rifting and volcanism in eastern China: a mantle dynamic link to the Indo-Asian collision? Tectonophysics, 393(1–4): 29–42

Mann P, Hempton M R, Bradley D C, Burke K (1983). Development of pull-apart basins. J Geol, 91(5): 529–554

Maruyama S, Isozaki Y, Kimura G, Terabayashi M (1997). Paleogeographic maps of the Japanese Islands: plate tectonic synthesis from 750 Ma to the present. Isl Arc, 6(1): 121–142

McClay K R, White M J (1995). Analogue modelling of orthogonal and oblique rifting. Mar Pet Geol, 12(2): 137–151

McCoss A M (1986). Simple constructions for deformation in transpression/transtension zones. J Struct Geol, 8(6): 715–718

Morley C K (2007). Variations in Late CenozoiceRecent strike-slip and oblique-extensional geometries, within Indochina: the influence of pre-existing fabrics. J Struct Geol, 29(1): 36–58

Morley C K, Haranya C, Phoosongsee W, Pongwapee S, Kornsawan A, Wonganan N (2004). Activation of rift oblique and rift parallel pre-existing fabrics during extension and their effect on deformation style: examples from the rifts of Thailand. J Struct Geol, 26(10): 1803–1829

Mortimer E, Paton D A, Scholz C A, Strecker M R, Blisniuk P (2007). Orthogonal to oblique rifting: effect of rift basin orientation in the evolution of the North basin, Malawi Rift, East Africa. Basin Res, 19(3): 393–407

Osagiede E E, Rotevatn A, Gawthorpe R, Kristensen T B, Jackson A L, Marsh N (2020). Pre-existing intra-basement shear zones influence growth and geometry of non-colinear normal faults, western Utsira high-heimdal terrace, North Sea. J Struct Geol, 130: 103908

Phillips T B, Fazlikhani H, Gawthorpe R L, Fossen H, Jackson C A L, Bell R E, Faleide J I, Rotevatn A (2019). The influence of structural inheritance and multiphase extension on rift development, the Northern North Sea. Tectonics, 38(12): 4099–4126

Pongwapee S, Morley C K, Won-in K (2019). Impact of pre-existing fabrics and multi-phase oblique extension on Cenozoic fault patterns, Wichianburi sub-basin of the Phetchabun rift, Thailand. J Struct Geol, 118: 340–361

Qi J F, Yang Q (2010). Cenozoic structural deformation and dynamic processes of the Bohai Bay Basin province, China. Mar Pet Geol, 27(4): 757–771

Qi J F, Yu F S, Lu K Z, Zhou J X, Wang Z Y, Yang Q (2003). Conspectus on Mesozoic basins in Bohai bay province. Earth Sci Front, 10(S1): 199–206 (in Chinese)

Ren J Y, Yu J G, Zhang J X (2009). Structures of deep bed in Jiyang Sag and their control over the development of Mesozoic and Cenozoic basins. Earth Sci Front, 16(4): 117–137 (in Chinese)

Schellart W P (2000). Shear test results for cohesion and friction coefficients for different granular materials: scaling implications for their usage in analogue modelling. Tectonophysics, 324(1–2): 1–16

Schlische R W, Withjack M O, Eisenstadt G (2002). An experimental study of the secondary deformation produced by oblique-slip normal faulting. AAPG Bull, 86(5): 885–906

Sun Z, Zhou D, Sun L T, Chen C M, Pang X, Jiang J Q, Fan H (2010). Dynamic analysis on rifting stage of Pearl River Mouth Basin through analogue modeling. J Earth Sci, 21(4): 439–454

Suo Y H, Li S Z, Peng G R, Du X D, Zhou J, Wang P C, Wang G Z, Somerville I, Diao Y X, Liu Z Q, Fu X J, Liu B, Cao X Z (2022). Cenozoic basement-involved rifting of the northern South China Sea margin. Gondwana Res, 120: 20-30

Suo Y H, Li S Z, Yu S, Somerville I D, Liu X, Zhao S J, Dai L M (2014). Genozoie tectonic jumping and implications for hydrocarbon accumulation in basins in the East Asia continental margin. J Asian Earth Sci, 88(1): 28–40

Thorkelson D (1996). Subduction of diverging plates and the principles of slap window formation. Tectonophysics, 255(1–2): 47–63

Tong H M, Cai D S, Wu Y P, Li X G, Li X S, Meng L J (2010). Activity criterion of pre-existing fabrics in non-homogeneous deformation domain. Sci China Earth Sci, 53(8): 1115–1125

Tron V, Brun J P (1991). Experiments on oblique rifting in brittle-ductile systems. Tectonophysics, 188(1–2): 71–84

Wang F W, Chen D X, Wang Q C, Shi X, Xie G, Wang Z, Li J, Liao W (2020). Evolution characteristics of transtensional faults and their impacts on hydrocarbon migration and accumulation: a case study from the Huimin Depression, Bohai Bay Basin, eastern China. Mar Pet Geol, 120: 104507

Wang G Z, Li S Z, Suo Y H, Zhang X Q, Zhang Z, Wang D Y, Liu Z, Liu Y J, Zhou J, Wang P C, Guo L L (2022). Deep-shallow coupling response of the Cenozoic Bohai Bay Basin to plate interactions around the Eurasian Plate. Gondwana Res, 102: 180–199

Wang L, Maestrelli D, Corti G, Zou Y Y, Shen C B (2021). Normal fault reactivation during multiphase extension: analogue models and application to the Turkana depression, East Africa. Tectonophysics, 811: 228870

Weijermars R, Schmeling H (1986). Scaling of Newtonian and non-Newtonian fluid dynamics without inertia for quantitative modelling of rock flow due to gravity (including the concept of Theological similarity). Phys Earth Planet Inter, 43(4): 316–330

Wu T J, Wu J (2019). Izanagi-Pacific ridge subduction revealed by a 56 to 46 Ma magmatic gap along the northeast Asian margin. Geology, 47(10): 953–957

Wu Z P, Hou X B, Li W (2007). Disscussion on Mesozoic basin patterns and evolution in the eastern North China block. Geotectonica et Metallogenia, 31(4): 385–399 (in Chinese)

Wu Z P, Hu Y, Zhong Z H (2015). Cenozoic faults characteristics and regional dynamic background of Panyu 4 subsag, Zhu I depression. J China U Petrol (Nat Sci Ed), 39(4): 1–9

Wu Z P, Li W, Ren Y J, Lin C S (2003). Basin evolution in the Mesozoic and superposition of Cenozoic basin in the area of the Jiyang depression. Acta Geol Sin, 77(2): 280–286 (in Chinese)

Yan J J, Wang X P (1996). On identification of wrench structure. Oil Gas Geol, 17(1): 8–11 (in Chinese)

Ye H, Shedlock K M, Hellinger S J, Sclater J G (1985). The North China basin: an example of a Cenozoic rifted intraplate basin. Tectonics, 4(2): 153–169

Yi X L, Hou G T (2002). A study of intensity of the faults activity in Jiyang depression in Mesozoic and Cenozoic. Acta Scientiarum Naturalium Universitatis Pekinensis, 38(4): 504–509 (in Chinese)

Zhan R, Yang G L, Zhang S, Zhu G (2012). Analysis on the origin of the composite flower structures in the Qingdong Sag. Geotectonica et Metallogenia, 36(4): 473–482 (in Chinese)

Zhang P, Wang L S, Ding Z Y, Zhong K (2006). Characteristics and formation mechanism of the faults in Mesozoic-Cenozoic in Jiyang Depression. Oil Gas Geol, 27(4): 467–474 (in Chinese)

Zhang W Z, Zhang Y Y, Zha M, Qu Z P,Yu J Q, Zhang L, He C (2019). Genetic model of transtensional faults in Dongying Depression, Bohai Bay Basin, and its controls over hydrocarbon accumulation. Oil Gas Geol, 40(2): 262–270 (in Chinese)

Zhao L, Li L (2016). The extensional pattern and dynamics of Bohai Bay basin in Late Mesozoic-Cenozoic. Geol China, 43(2): 470–485 (in Chinese)

Zhao L, Li L (2017). The relationships between normal fault and strike-slip fault in Jiyang depression. Geol Rev, 63(1): 50–60 (in Chinese)

Zhao Y J (2007).The research of basin structure and filling characteristics of Palaeogene in Dongying depression. Guangzhou, China: Guangzhou Institute of Geochemistry of the Chinese Academy of Sciences, 34–73 (in Chinese)

Zheng D S, Wu Z P, Li W, Zhou Y Q (2005). Basin evolution in the Mesozoic and superposition of Cenozoic basin in the area of the Jiyang depression. Acta Geol Sin, 79(3): 386–394 (in Chinese)

Zhong D L, Ding L, Ji J Q, Zhang J J, Liu F T, Liu J H, Yan X W (2001). Coupling of the lithospheric convergence of west China and dispersion of east China in Cenozoic: link with paleoenvironmental changes. Quat Sci, 21(4): 303–312 (in Chinese)

Zhu G, Liu C, Gu C C, Zhang S, Li Y J, Su N, Xiao S Y (2018). Oceanic plate subduction history in the western Pacific Ocean:

constraint from late Mesozoic evolution of the Tan-Lu Fault Zone. Sci China Earth Sci, 61(4): 386–405

Zhu G, Liu G S, Niu M L, Song C Z, Wang D X (2003). Transcurrent movement and genesis of the Tan-Lu fault zone. Geol Bull China, 22(3): 200–207 (in Chinese)

Zong G H, Xiao H Q, Li C B, Shi Y S, Wang L S (1999). Evolution of Jiyang depression and its tectonic implications. Geol J China U, 5(3): 275–282 (in Chinese)